



Analytical Methods

Novel non-invasive distribution measurement of texture profile analysis (TPA) in salmon fillet by using visible and near infrared hyperspectral imaging

Di Wu^a, Da-Wen Sun^{a,*}, Yong He^b^a Food Refrigeration and Computerised Food Technology (FRCFT), School of Biosystems Engineering, University College Dublin National University of Ireland, Agriculture and Food Science Centre, Belfield, Dublin 4, Ireland^b College of Biosystems Engineering & Food Science, Zhejiang University, Hangzhou 310058, Zhejiang, PR China

ARTICLE INFO

Article history:

Received 31 July 2012

Received in revised form 8 March 2013

Accepted 14 August 2013

Available online 27 August 2013

Keywords:

Hyperspectral imaging

Optimal wavelength

Texture profile analysis (TPA)

Imaging spectroscopy

Salmon

Fish

ABSTRACT

This study developed a pushbroom visible and near-infrared hyperspectral imaging system in the wavelength range of 400–1758 nm to determine the spatial distribution of texture profile analysis (TPA) parameters of salmon fillets. Six TPA parameters (hardness, adhesiveness, chewiness, springiness, cohesiveness, and gumminess) were analysed. Five spectral features (mean, standard deviation, skew, energy, and entropy) and 22 image texture features obtained from graylevel co-occurrence matrix (GLCM) were extracted from hyperspectral images. Quantitative models were established with the extracted spectral and image texture signatures of samples based on partial least squares regression (PLSR). The results indicated that spectral features had better ability to predict TPA parameters of salmon samples than image texture features, and Spectral Set I (400–1000 nm) performed better than Spectral II (967–1634 nm). On the basis of the wavelengths selected by regression coefficients of PLSR models, instrumental optimal wavelengths (IOW) and predictive optimal wavelengths (POW) were further chosen to reduce the high dimensionality of the hyperspectral image data. Our results show that hyperspectral imaging holds promise as a reliable and rapid alternative to traditional universal testing machines for measuring the spatial distribution of TPA parameters.

© 2013 Elsevier Ltd. All rights reserved.

1. Introduction

Texture of the raw flesh is a critical quality attribute that is relevant to the overall quality and acceptability of fish product (Sigurgisladdottir et al., 1999; Veland & Torrisen, 1999). This attribute is affected by the connective tissue and the myofibrils in fish flesh. The connective tissue is composed of mainly collagen that is responsible for tensile strength, while the myosin and actin are the main constituents for myofibrils (Casas, Martinez, Guillen, Pin, & Salmeron, 2006). The manner in which the muscle tissue handles and feels in the mouth is affected by the textural features, which come from the properties and concentrations of the tissue components and their complicated arrangement in the muscle (Dunajski, 1979). A salmon product with soft flesh has an unpleasant mushy mouthfeel and will reduce acceptability by the consumers, leading to a quality downgrading for this product in the fish processing industry (Ashton, Michie, & Johnston, 2010; Morkore & Einen, 2003). Besides being relevant to mouthfeel, texture is also a general quality property related to freshness (Isaksson, Swensen,

Taylor, Fjaera, & Skjervold, 2002). A reliable method for determining salmon muscle texture is important in establishing quality grades for the salmon industry (Isaksson et al., 2002), and is also critical in the development of optimal farming conditions, feeding regimes and proper handling procedures for producing salmon products with a prime eating quality (Dunajski, 1979; Veland & Torrisen, 1999).

There are two main approaches to determining the texture of salmon flesh: organoleptic/sensory assessment using trained panels and instrumental analysis (Dunajski, 1979; Isaksson et al., 2002). “Finger method” is a commonly used touch method in the industry to test texture of raw salmon fillets (Sigurgisladdottir et al., 1999). The firmness of texture is indicated on rating scales, which are given with points anchored verbally by the panelists (Dunajski, 1979). The designer and executor of sensory assessment should have adequate technical ability and experience to get trustworthy outputs (Ashton et al., 2010). The sensory tests are dependent to a great extent on subjective and inconsistent assessment of the panelist (Sigurgisladdottir et al., 1999). The processes of sensory tests are also tedious, time-consuming, and costly. There is another limiting factor that it is not feasible to compare results from laboratory to laboratory or from batches to batches assessed in the same laboratory directly (Ashton et al., 2010). On the other hand,

* Corresponding author. Tel.: +353 1 7167342; fax: +353 1 7167493.

E-mail address: dawen.sun@ucd.ie (D.-W. Sun).URLs: <http://www.ucd.ie/refrig>, <http://www.ucd.ie/sun> (D.-W. Sun).

mechanical measurement methods can obtain objective results for evaluating texture of salmon fillets in a low cost way (Sigurgisla-dottir et al., 1999). If a strict standardisation is strictly controlled for the mechanical measurement, its output results could be comparable between laboratories or batches from the same laboratory (Ashton et al., 2010). Compared with sensory evaluations, mechanical measurements have little influence by human factors so that the variation among measurements could be reduced (Casas et al., 2006). However, although objective and consistent, instrumental measurements cannot be used routinely by the industry, because they are time-consuming, destructive, and inefficient. Moreover, both sensory assessment and instrumental analysis are selective examinations, which can only evaluate small numbers of samples. The salmon industry requires the development of a non-destructive means of texture evaluation method and incorporation of the method with the existing salmon grading protocols to establish prime quality grades.

Recently, visible and near infrared (Vis–NIR) spectroscopy has been successfully proved to be one of the most efficient and advanced tools for non-destructive analysis and control for food quality (Chen, Wu, He, & Liu, 2011; Wu, He, Feng, & Sun, 2008b; Wu et al., 2011; Abdel-Nour, Ngadi, Prasher, & Karimi, 2011; Francesca et al., 2011). Particularly for texture analysis of salmon, Isaksson et al. (2002) assessed texture of farmed Atlantic salmon using Vis–NIR spectroscopy. However, they found that no prediction of texture profile analysis (TPA) value was possible. The lack of precision might be due to that TPA technique only measured a small area of inhomogeneous muscle, and the sampling positions of TPA and Vis–NIR spectral measurements were not the same. In their work, no significant ($p > 0.05$) correlation was found between two TPA measurement points in one fillet, which showed that there was a texture variation along the fillet. Such variation in textural property is due to the varying of chemical constituents and physical structure of the muscle along the fillet (Jonsson, Sigurgisla-dottir, Hafsteinsson, & Kristbergsson, 2001). Therefore, sampling is an important factor for both instrumental measurements and Vis–NIR spectroscopy in the evaluation of salmon fillet texture because of the heterogeneity of the fillets. The measurements of textural properties using above mentioned methods depend on the location within the fillet, indicating that the sampling position is critical for the point detection methods for assessing salmon fillet texture. Moreover, the distribution of texture is an important quality attribute of salmon (Casas et al., 2006). Rapid and quantitative measurement of texture distribution can significantly improve process efficiency as salmon could be trimmed into different quality grades based on consumer requirements.

Measurement of the attribute distribution of food could be achieved by hyperspectral imaging technique which offers the feasibility of measuring the complete wavelength spectrum over the visible and near-infrared wavelengths in terms of millions of pixels simultaneously. On the basis of its simultaneously measured spectral and spatial information, hyperspectral imaging can capture both physical and morphological characteristics such as colour, size, shape, and texture, and the distribution of some intrinsic chemical and molecular information (such as water, fat, and protein) from a food product. As a rapid and non-invasive technique for quality evaluation, hyperspectral imaging would let salmon processing industries and others to be able to inspect all or many fillets instead of using only small sample for selective tests, like sensory test and instrumental measurement. In recent years, new advances in hyperspectral imaging make this technique become a powerful extension of both spectroscopy and imaging techniques or computer vision (Sun, & Brosnan, 2003; Du, & Sun, 2005; Jackman, Sun, Du, & Allen, 2008; Wang, & Sun, 2002; Valous, Mendoza, Sun, & Allen, 2009; Jackman, Sun, Du, & Allen, 2009) for the non-destructive measurement of quality distribution in a

wide range of applications (He, Wu, & Sun, 2013; Lorente, Aleixos, Gómez-Sanchis, Cubero, & Blasco, 2013; Lorente et al., 2012; Wu et al., 2013).

Fish muscles have a characteristic metameric structure, which is quite uncommon in mammalian tissues (Dunajski, 1979). The key factors influencing the variations in salmon texture are the muscle structure such as connective tissue (myocommata) and biochemical properties such as moisture content, the liquid neutral lipids, and myofibrillar proteins. Image texture was found to have relationship with muscle structure (Zheng, Sun, & Zheng, 2006a), while spectra were used to relate spectral reflectance measurements to biochemical properties of fish muscle (Berzaghi & Riovan-to, 2009). Therefore, it is of our interest to investigate the feasibility of using image texture features and spectral features extracted from hyperspectral images for determining texture in salmon fillet. To the best of our knowledge, this is the first study on using hyperspectral imaging to measure texture distribution of salmon fillets. The overall objective of this study was to investigate the potential of Vis–NIR hyperspectral imaging in the spectral range of 400–1753 nm for the rapid and non-invasive measurement of texture distribution of salmon fillets. The successful outcome of the study is very advantageous to assure buyers and consumers of salmon products of consistently high quality. The work was conducted by (1) establishing a hyperspectral imaging system in the spectral region of 400–1753 nm to acquire Vis–NIR hyperspectral images of salmon fillets, (2) extracting image texture and spectral features from hyperspectral images, (3) comparing the determination abilities of two spectral sets of 400–1000 and 897–1753 nm, (4) identifying optimal wavelengths that are most useful for the prediction of TPA parameters within salmon fillets and can be used for designing a multispectral imaging system, (5) establishing multivariate analysis models based on image texture and spectral features, and (6) displaying the texture distribution in salmon fillets by predicting TPA parameters of each pixel in the image.

2. Materials and methods

2.1. Samples preparation

Three groups (24 fillets in all) of fresh farmed Atlantic salmon fillets (*Salmo salar*) were purchased from local supermarkets in Dublin, Ireland (ten fillets from Scotland, eight fillets from Norway, and six fillets from Ireland). The salmon fillets were fresh and of superior quality. The fillets were labelled and then transported to the laboratories of Food Refrigeration and Computerized Food Technology (FRCFT), University College Dublin (UCD), Ireland. Each fillet was first scanned by the hyperspectral imaging system and then its reference values of TPA parameters were determined using a universal testing machine as explained below.

2.2. Hyperspectral imaging system

There were two hyperspectral imaging systems used in this study for the acquisition of hyperspectral images of each fillet. The working spectral ranges of two systems were 400–1000 nm (System I) and 897–1753 nm (System II). System I (DV optics, Padua, Italy) mainly consisted of a Specim V10E spectrograph (Spectral Imaging Ltd., Oulu, Finland) covering the spectral range of 400–1000 nm (spectroscopic resolution of 5 nm), a high performance CCD camera (Basler A312f, effective resolution of 580×580 pixels by 12 bits), an objective lens (25 mm focal length), an illumination source (150 W halogen lamp source attached to a fibre optic line light positioned at an angle of 45° to the moving table), a mirror, a moving table, an computer system equipped with an acquisition software (Spectral Scanner, DV Optics, Padua, Italy). A diffuse light source was produced by placing a cylindrical diffuser in front of the

fibre optic line light. The main components of System II include a 12-bit CCD camera (320 spatial \times 256 spectral photodiodes) along with focusing lens (Xeva 992, Xenics Infrared Solutions, Leuven, Belgium), a spectrograph (ImSpector N17E, Specim, Spectral Imaging Ltd., Oulu, Finland), an illumination unit consisting of two 500 W halogen lamps (ViP V-light, Lowell Light Inc., NY, USA) fixed above the sample from both sides at an angle of 45° and at the height of 60 cm to reduce the shadowing effects, a moving table operated by a stepper motor (GPL-DZTSA-1000-X, Zolix Instrument Co. Ltd., Beijing, China) and a computer supported with Spectra-Cube data acquisition software (Spectral Imaging Ltd., Oulu, Finland).

In experiment, each fillet was placed on the moving table of each system and then was scanned line by line to acquire the hyperspectral images in 400–1000 and 897–1753 nm, respectively. The acquired images were then corrected into reflectance images according to the method used by Wu et al. (2012b). Due to decreased CCD detector sensitivity in the wavelength regions of 897–967 and 1634–1753 nm, subsequent analysis of hyperspectral images acquired by System II was performed only on data in the 967–1634 nm spectral range. Finally, two sets of spectral data were obtained, which were the one within the wavelength ranges of 400–1000 nm (Spectral Set I, 121 wavelength variables) and the one within the wavelength ranges of 967–1634 nm (Spectral Set II, 200 wavelength variables).

2.3. Subsampling and TPA reference analysis

The texture can vary much along the fillet and texture at different positions within the fillet could be different. On the other hand, the development of the calibration model requires an appropriate span of attribute values in the calibration samples (Berzaghi & Riovanto, 2009). This was done by cutting out samples (rectangular shapes with dimensions of 2 \times 2 \times 1.5 cm) from different locations of every fillet, resulting in a total of 120 samples for texture profiles analysis (TPA). Wide variation in texture was provided by subsampling for establishing multivariate calibration models that could be applied for pixel-wise visualisation of texture distribution.

TPA of samples was measured by using an Instron universal testing machine (Model 4411, Canton, Mass, USA). Each cut sample was compressed twice to 60% of their original height at 100 mm/min speed and 100 N compression load using a cylindrical-shaped probe (50 mm in diameter). The probe re-penetrated the fillet 10 s after the first compression cycle. The most common parameters derived from the TPA curve are hardness, adhesiveness, chewiness, springiness, cohesiveness, and gumminess, which were calculated according to the method of Bourne (2002).

2.4. Object measurement

Intensity-based/spectral data extraction and texture-based extraction are two main categories of object measurement. On the basis of the object measurement, quantitative spectral models were established through multivariate data analysis and used for further texture prediction of each pixel and generation of texture distribution map. The establishment of quantitative models requires the regions for extracting object features have the same position and shape of the sample whose TPA parameters were measured by the Instron universal testing machine. Otherwise, such establishment would be not meaningful. In this study, the region of interests (ROI) function of ENVI v4.6 software was used to isolate the ROIs of sample from the images of fillets manually. After identification of ROIs, the object measurement was conducted from each sample in hyperspectral images.

2.4.1. Spectral data extraction

Mean spectrum of ROI is the most widely used spectral data extraction. It is calculated by averaging the spectrum of pixels within the ROI at each wavelength to obtain one mean value representing the ROI. Besides mean, the first-order measures also include standard deviation, skew, energy, and entropy. Detailed functions of these algorithms can be found elsewhere (Umbaugh, 2010). All these five features were extracted in this study for both Spectral Sets I and II.

Salmon muscle mainly consists of the connective tissues of the myocommata which are usually shown in white and the myotomes which are segmented by myocommata and shown in red/pink. Fat deposits also contribute to the white colour. Therefore, besides the extraction of mean spectrum of the whole ROI, the mean spectra of myocommata and fat deposits (Area I) and myotomes (Area II) were also extracted for the texture determination. To conduct such extraction from ROI in the hyperspectral image, the segmentation process was developed to separate Area I and Area II with the aid of self-developed programs in the Matlab 2011a software. In order to select optimal wavelengths for the segmentation of hyperspectral images in Spectral Sets I and II, respectively, the typical spectra of Areas I, II, and whole ROI are shown in Fig. 1. The wavelengths 495 and 974 nm had the maximum abilities to generate the segmented masks for separating Area I from Area II in Spectral Sets I and II, respectively. The mean spectra of Area I and Area II in each ROI were then obtained based on the segmented masks.

2.4.2. Image texture extraction

Image texture is an important image feature and has been applied greatly in the food industry for quality evaluation and inspection (Zheng, Sun, & Zheng, 2006b). Graylevel co-occurrence matrix (GLCM) is a mostly used statistical texture analysis method, which extracts texture features from the co-occurrence matrix, $p(k, l)$ (Haralick, Shanmuga, & Dinstein, 1973). The establishment of co-occurrence matrix requires two parameters θ (direction of the pixel pairs) and d (distance between the pixel pairs). In this study, 22 GLCM features were extracted, which were uniformity/energy/angular second moment, entropy, dissimilarity, contrast/inertia,

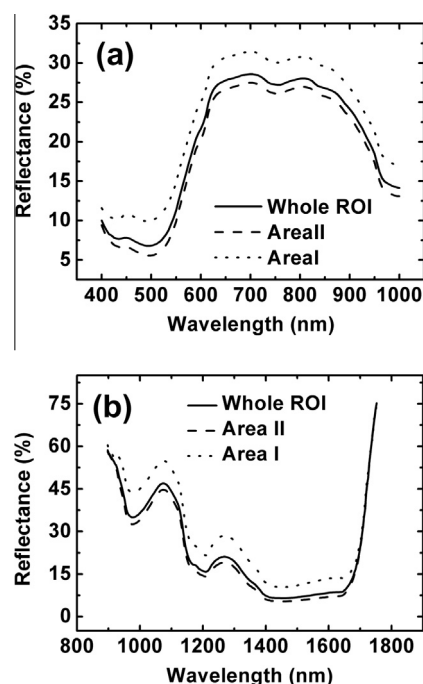


Fig. 1. Extracted mean spectral features of area I (myocommata and fat deposits), area II (myotomes), and whole ROI. (a) 400–1000 nm, (b) 967–1634 nm.

inverse difference, correlation, homogeneity/inverse difference moment, autocorrelation, cluster shade, cluster prominence, maximum probability, sum of squares, sum average, sum variance, sum entropy, difference variance, difference entropy, information measures of correlation-I, information measures of correlation-II, maximal correlation coefficient, inverse difference normalized (INN), and inverse difference moment normalized (IDN). The calculation functions of these features are shown in the references (Clausi, 2002; Haralick & Shanmuga, 1973; Soh & Tsatsoulis, 1999). The above feature extraction considered four different θ values of 0°, 45°, 90°, and 135° and three d values of 1, 3, and 5 pixels. There were three strategies considered in this study to extract GLCM features. The first strategy extracted GLCM features from images at every wavelength over the full range (Strategy I), the second one extracted GLCM features from the principal component images (Strategy II) that were obtained by conducting principal component analysis (PCA), and the third one extracted GLCM features from images only at optimal wavelengths (Strategy III).

2.5. Data analysis

2.5.1. Optimal wavelength selection

The current hyperspectral imaging system has not been available for implementation in salmon processing lines but only used in laboratory-based analysis, because its data acquisition is relatively slow and hyperspectral image data are too complicated to be calibrated directly. The selection of the most optimal wavelengths needs to be conducted to speed up the acquisition of hyperspectral images and optimise subsequent analysis process. In this study, the regression coefficients resulting from the PLSR calibration models with full spectral range were used to choose the most optimal wavelengths that had less redundancy and contributed most in texture determination of the salmon samples. A variable (wavelength) corresponding to a large regression coefficient value (regardless of the sign) was interpreted as a relevant candidate for the considered predictive model. In this study, the calibration in the way that uses the full spectral range (121 wavelengths for Spectral Set I and 200 wavelengths for Spectral Set II) was called Method I; while utilizing only the optimal wavelengths selected by regression coefficients for specific TPA parameter was called Method II throughout this paper.

2.5.2. Multivariate data analysis

Due to the huge amount of spectral and image textural features that could be extracted from hyperspectral images, multivariate data analysis is required to correlate the multiple variables of extracted feature data to the reference values of quality attributes. The extracted features of each sample was arranged together to form a matrix which consisted of a feature matrix (X) of n features (n depends on specific analysis) \times 120 samples as independent variables and a column vector (Y) containing the measured reference values of TPA parameter of the samples as dependent variables. Multivariate data analysis was then aimed to establish quantitative model between the spectral matrix (X) and column vector (Y).

In this study, partial least squares regression (PLSR) was used to perform calibrations and predictions of TPA parameters in salmon samples based on the extracted hyperspectral image features. PLSR is a classical method for multivariate data analysis and has been applied in many spectral analyses (Antonucci et al., 2011; Chen & Lei, 2009; Hu, Toyoda, Yamanoue, Ihara, & Nakai, 2010; Siniša & Mishra, 2011; Wu, He, Nie, Cao, & Bao, 2010). In PLSR calculation, a set of orthogonal factors called 'latent variables' (LVs) is projected from the spectral data. The optimal number of LVs depends on the prediction error, typically done by using the lowest value of the predicted residual error sum of squares (PRESS). As a chemometric method, PLSR is usually used to reduce multi-collinearity existed in

spectra, which commonly include several hundreds of wavelength variables. It is not required to use PLSR in the case with a small number of variables, such as the selected optimal wavelengths. Multiple linear regression (MLR) is a commonly used calibration algorithm, which builds a relationship between independent variables and dependent variables in the form of a linear equation. However, MLR requires that input variables have less number than that of samples. Therefore, it is not possible to run MLR directly on the full range spectra, because the number of predictors is usually more than that of samples. The optimal variable selection is required before the MLR model establishment.

2.5.3. Model evaluation

The predictive ability of the calibration model was evaluated by correlation coefficients of calibration (r_c) and root mean square error of calibration (RMSEC). Besides calibration, leave-one-out cross validation (LOOCV) was used for the validation purpose during the calibration process of quantitative model. Correlation coefficients of cross-validation (r_{cv}) and root mean square error of cross-validation (RMSECV) were used to evaluate the performance of validated model. Generally, a good model should have high correlation coefficients (r_c and r_{cv}) and low root mean square error (RMSEC and RMSECV) as well as a small difference between RMSEC and RMSECV.

2.6. Visualization of TPA distribution

As the replacement of the measurement of average concentration for detailed quality analysis, the distribution maps of quality attributes have the advantages of knowing and understanding the heterogeneity of salmon products. Because each pixel in the hyperspectral image has its own spectrum with its spatial position, the intensities of quality attributes, such as texture in this study, can be predicted at each pixel by inputting its spectrum into the established quantitative model. Because it is practically impossible to obtain the reference values of attributes for every pixel using reference analysis, the quantitative model was established using the extracted image features of the sample within the ROI, on which the reference value was available to be measured. A distribution map of texture within the whole fillet can then be generated based on the spatial position of every pixel and the corresponding colour values. All of the computations, chemometric analyses and visualization process were operated with ENVI 4.6 (Research System, Inc., USA), "The Unscrambler V9.7" (CAMO PROCESS AS, Oslo, Norway), and programs developed by us in the Matlab 2011a software (The Mathworks, Inc., Natick, MA, USA).

3. Results and discussion

3.1. Statistics of measured TPA parameters

The establishment of a robust calibration model requires a reasonable range of quality variation for the calibration samples, whereas a narrow range can negatively affect predictability of any quality attributes (ElMasry, Sun, & Allen, 2012). Table 1 summarises the relevant statistics of six TPA parameters for the examined salmon samples. The presence of a broad range of TPA parameters indicated that the tested samples had a good representation to build realistic calibration models. Because gumminess is defined as the product of hardness \times cohesiveness and chewiness is defined as the product of gumminess \times springiness (which is hardness \times cohesiveness \times springiness) (Bourne, 2002), the results of their calculation from TPA parameters (Process I) and the values predicted directly from hyperspectral images (Process II) were compared to establish a better way for determining these two parameters.

Table 1

Reference results of TPA parameters of salmon samples measured by the Universal testing machine.

TPA parameter	Max	Min	Mean \pm SD ^a	Range
Hardness	29.127	2.212	10.97 \pm 5.46	26.915
Cohesiveness	0.705	0.270	0.52 \pm 0.08	0.435
Adhesiveness	3.454	0.243	1.60 \pm 0.63	3.211
Springiness	5.880	2.530	4.53 \pm 1.07	3.350
Gumminess	12.330	1.217	5.50 \pm 2.60	11.113
Chewiness	72.061	3.079	25.94 \pm 15.70	68.982

^a SD = Standard Deviation.

3.2. Spectral features of salmon fillets

The typical spectral pattern of salmon sample in two spectral sets is shown in Fig. 1. For salmon fillets, the spectral profiles are quite even with some broadband peaks in whole spectral region. There were high reflectance values at the red range in the visible spectral region (400–700 nm), which makes salmon with red colour. In the near infrared spectral region (700–1700 nm), some absorption peaks were found in the spectral patterns of the salmon fillet. The presence of water in the salmon fillet caused three absorption peaks appeared at 760 nm (O–H stretching third overtone) in Fig. 1a and 980 and 1450 nm (O–H stretching second and first overtones) in Fig. 1b. Another local absorption maximum appeared at 1220 nm was due to C–H stretching second overtone of fat. Beside, protein information is hidden around 1500 nm (N–H stretching first overtone), which was immersed in the absorption of water.

3.3. Calibration of TPA parameters based on full spectral range

By setting the mean reflectance spectra extracted from all samples as the predictors and their corresponding TPA parameter values as the target values, PLSR was conducted to establish quantitative models based on Spectral Sets I and II, respectively. Table 2 shows the statistical parameters of PLSR models in calibration and cross-validation processes for the determination of six TPA parameters. When Spectral Set I was considered, the PLSR models for determining four TPA parameters (hardness, adhesiveness, gumminess, chewiness) had r_c higher than 0.7 and r_{cv} higher

than 0.6. Meanwhile prediction of springiness was not satisfactory, for which r_c and r_{cv} were only 0.464 and 0.369. Gumminess and chewiness were also calculated based on the values of hardness, cohesiveness and springiness, which were predicted based on PLSR models (Process I). The RMSEC and RMSECV of the gumminess model established based on PLSR model were lower than those of gumminess values calculated from predicted hardness and cohesiveness. For chewiness analysis, Process I and Process II had similar results. When Spectral Set II was considered, the r_{cv} values of PLSR models for determining cohesiveness and springiness were lower than 0.4 and those of other four TPA parameters were between 0.45 and 0.6. Although long-wave near infrared spectra (Spectral Set II) contain more information relevant to hydrogen containing bonds than visible and short-wave near infrared spectra (Spectral Set I), the calibration and validation results of PLSR models established with Spectral Set I were better than those with Spectral Set II. This might be because the salmon samples contained much water content, which caused the information of other components being immersed in the absorption of water in Spectral Set II. The effect of intense water bands in the long-wave near infrared spectral region can be diminished in short-wave near infrared spectral region (Reeves, 1994). This was the first time that two most general spectral ranges of hyperspectral imaging systems were compared. Besides mean spectrum, other four first-order measures (standard deviation, skew, energy, and entropy) were also considered as the predictors of PLSR models. However, the results of these four first-order measures were not as good as those of mean spectrum. When Spectral Set I was considered, the best r_{cv} values were 0.486 (standard deviation) for hardness, 0.326 (standard deviation) for cohesiveness, 0.539 (standard deviation) for adhesiveness, 0.153 (energy) for springiness, 0.437 (entropy) for gumminess, and 0.308 (entropy) for chewiness, respectively. When Spectral Set II was considered, cohesiveness and adhesiveness had similar results compared to those of Spectral Set I and other TPA parameters were poorer (data not shown). In addition, the mean spectra of Area I and Area II were used to establish the quantitative relationships with TPA parameters. When Spectral Set I was considered, the best r_{cv} values were 0.439 (Area II) for hardness, 0.444 (Area I) for cohesiveness, 0.614 (Area II) for adhesiveness, 0.215 (Area I) for springiness, 0.443 (Area II) for gumminess, and 0.396 (Area II) for chewiness, respectively. It is noticed

Table 2

Partial least square regression (PLSR) models for predicting texture (hardness, cohesiveness, adhesiveness, springiness, gumminess, and chewiness) of salmon samples by using the mean spectra of ROI in full spectral range (Method I).

Spectral Set	Texture	No. of latent variable	Calibration		Cross-validation	
			r_c	RMSEC	r_{cv}	RMSECV
I	Hardness	8	0.734	3.689	0.665	4.091
	Cohesiveness	8	0.648	0.060	0.555	0.067
	Adhesiveness	11	0.727	0.432	0.606	0.504
	Springiness	4	0.464	0.944	0.369	0.999
	Gumminess	10	0.754	1.701	0.665	1.952
	Gumminess ^a	/	0.713	1.821	0.633	2.012
	Chewiness	8	0.704	11.109	0.605	12.559
	Chewiness ^b	/	0.695	11.320	0.616	12.320
II	Hardness	11	0.742	3.640	0.526	4.659
	Cohesiveness	12	0.686	0.058	0.347	0.075
	Adhesiveness	6	0.668	0.467	0.578	0.517
	Springiness	4	0.470	0.940	0.389	0.990
	Gumminess	10	0.518	2.217	0.457	2.325
	Chewiness	8	0.523	13.322	0.470	13.914

^a Calculated from the definition of gumminess (the product of hardness \times cohesiveness), where the values of hardness and cohesiveness were predicted based on PLSR models (Process I).

^b Calculated from the definition of chewiness (the product of hardness \times springiness), where the values of hardness, cohesiveness and springiness were predicted based on PLSR models (Process I).

that the prediction of adhesiveness by using the mean spectra of Area II had similar result as that of whole salmon fresh, whereas the extraction of the mean spectra of Area I and Area II in Spectra Set I had little improvement of determination of other TPA parameters. When Spectral Set II was considered, the mean spectra of Area II had better results than those of Area I for all six TPA parameters. When it was compared between two Spectral Sets, similar results were obtained by two Spectral Sets for hardness, gumminess, and chewiness, while Spectral Set I had better determination for adhesiveness, and cohesiveness and springiness were better predicted by Spectral Set II.

Besides the analysis of spectral features, image texture was also extracted based on the calculation of GLCM within hyperspectral images. The average results of four different angles namely 0°, 45°, 90°, and 135° were used to eliminate the effect of rotation variance (Du & Sun, 2006). The 22 second-order textural feature were extracted from full spectral range (Strategy I), resulting in $22 \times 121 = 2662$ features for Spectral Set I and $22 \times 200 = 4400$ features for Spectral Set II for different d values. However, no matter what Spectral Set and d value were considered, the established PLSR models were not satisfactory (data not shown). For Spectral Set I, different d values had similar results, while d of 1 was better than other two d values for Spectral Set II. The extraction of image textural features was also reported by using GLCM from PC images (Naganathan et al., 2008b). In this study, PCA was first implemented to reduce the spectral dimension and GLCM was then used to extract image textural features from the first eight PC images (Strategy II), resulting in $22 \times 8 = 176$ features for Spectral Set I and Spectral Set II, respectively. Three d values were also considered in Strategy II. However, the performances of Strategy II were poorer than those of Strategy I for all six TPA parameters (data not shown). Similar results were obtained for different d values in Strategy II, and Spectral Set II was poorer than Spectral Set I.

It can thus be confirmed that hyperspectral imaging can be used for determining texture of salmon fillets in a rapid and non-invasive way. On the basis of spatial information within hyperspectral images, quantitative relationships were established between the extracted spectral features and TPA parameters. Compared to previous study in which no spectral prediction of TPA was possible (Isaksson et al., 2002), the prediction results of spectral models were much improved in the current study. Furthermore, the exact texture of a sample is usually not concerned by the salmon manufacturers, who would be on the contrary more likely to know which texture subgroup that the sample belongs to (e.g., high hardness and low hardness). In this study, a classification accuracy of 92.5% was achieved by using partial least square discriminant analysis (PLS-DA) (Wu, Feng, He, & Bao, 2008a), when samples were classified into two subgroups: high hardness values (hardness >16) and low hardness values (hardness <16).

3.4. Identification of optimum wavelengths

Because Spectral Set I had better results than Spectral Set II, only the spectral range of 400–1000 nm (Spectral Set I) was considered in the identification of optimum wavelengths. According to previous researches (Wu, Chen, Zhu, Guan, & Wu, 2011; Wu, He, Shi, & Feng, 2009), equal or better results were obtained based on the selected optimal wavelengths compared to full wavelengths, which was because they carry the most important information relevant to the determination. In this study, ten (hardness), nine (cohesiveness), eleven (adhesiveness), ten (gumminess), and ten (chewiness) wavelengths were identified as the optimal wavelengths by using the regression coefficient method. The selection of optimum wavelengths was not conducted for springiness, as its determination was not good in this study. Fig. 2 shows the calculated regression coefficients of PLSR models

(Method I) for different TPA parameters. Some strong peaks and valleys (positive and negative relationships with the TPA parameters) were selected at certain wavelengths and are highlighted in Fig. 2. Table 3 shows the performance of PLSR models established by using the selected optimal wavelengths (mean spectra in Spectral Set I) for five TPA parameters. The simplified PLSR models (Method II) had similar results to the original models (Method I). Except the increase of 4.08% for RMSECV of cohesiveness model (Method II), the RMSECV values of other four models (Method II) decreased 5.89% (hardness), 3.47% (adhesiveness), 6.75% (gumminess), and 7.23% (chewiness), respectively. Moreover, the absolute differences between RMSEC and RMSECV of PLSR models (Method II) were only 49.29% (hardness), 72.07% (cohesiveness), 58.73% (adhesiveness), 55.49% (gumminess), and 33.20% (chewiness) of those of PLSR models (Method I), showing that the wavelength selection could make the reduced models more stable and robust.

Currently, the wavelength selections in most studies of spectral analysis were conducted respectively for each individual quality trial (ElMasry et al., 2012; Wu, Nie, He, & Bao, 2012a). When a multispectral imaging system is designed for determining several quality trials, there will be still many band-pass filters required to obtain the spectra at the selected wavelengths of these trials. In this study, after the elimination of repeated wavelengths, there were still 28 wavelengths for the determination of five TPA parameters (without springiness). So many wavelengths would make the reduced spectral matrix remaining very large, resulting in a meaningless of the wavelength selection. Therefore, on the basis of 28 wavelengths selected in Method II, a further selection process was conducted to reduce the wavelengths with keeping the performances of models as much as possible (Method III). As a result, a new optimal wavelength set was selected, which had 14 wavelengths (405, 410, 460, 515, 555, 560, 580, 615, 735, 865, 920, 945, 955, and 990 nm). With the further selected wavelengths (called instrumental optimal wavelengths, IOW), the number of band-pass filters would be reduced by 50.00% from 28 to 14, which is important for designing a simple multispectral imaging system to meet the speed requirement of real-time production lines. The results of PLSR models (Method III) as shown in Table 3 were close to those of Method II. The changes of RMSECV values were 6.43%, –4.61%, 1.28%, 2.13%, and 1.91% for the determination of hardness, cohesiveness, adhesiveness, gumminess, and chewiness, respectively.

Furthermore, the measured spectra at IOW using band-pass filters might not be all required for predicting each TPA parameter. In order to further optimize PLSR models for the determination of TPA parameters, the predictive optimal wavelengths (POW) were further selected by reducing the number of IOW with keeping the performances of models as much as possible (Method IV). There were eleven POW for adhesiveness and ten POW for hardness, cohesiveness, gumminess, and chewiness, respectively (Specific wavelength values could be found in Eqs. (1)–(5) as shown later). Table 3 shows the main statistics of the PLSR models developed with POW. The final PLSR models (Method IV) with POW had comparable results to previous PLSR models (Methods I, II, and III). Compared to the results of Method I (Table 2), the RMSECV were reduced by 0.94–10.61% with an average of 5.33% and the absolute differences between RMSEC and RMSECV were reduced by 9.75–62.38% with an average of 42.97% for the determination of five TPA parameters (without springiness). As a fewer wavelengths were chosen in PLSR models (Method IV) compared to Method III, POW were considered as the final optimal wavelengths for the TPA determination. Besides the establishment of PLSR models (Method IV), MLR was also considered for the determination of TPA parameters based on POW, since MLR equations are simple and easy to interpret. In this study, the obtained MLR equations for predicting TPA parameters are shown as follows:

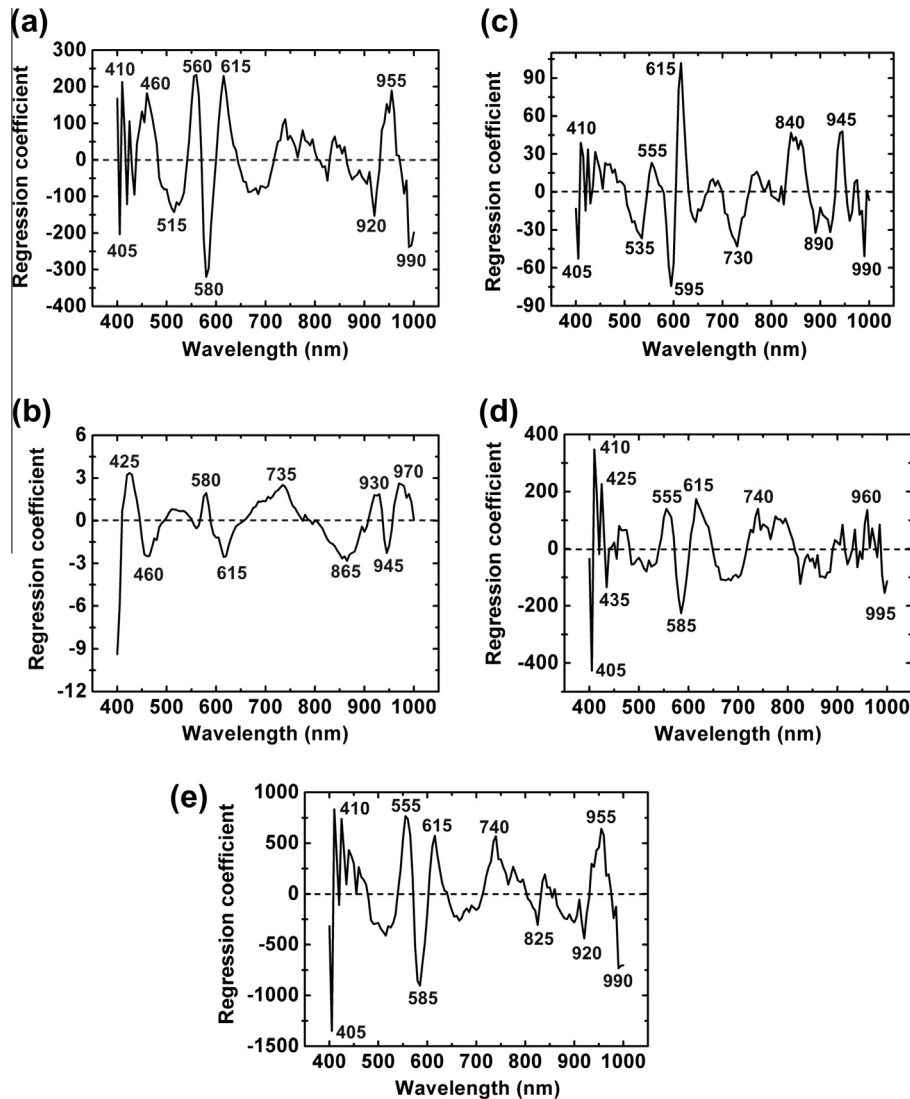


Fig. 2. Selection of optimal wavelengths. Regression coefficients of PLSR models (Method I) for (a) hardness, (b) cohesiveness, (c) adhesiveness, (d) gumminess, and (e) chewiness of salmon samples.

$$Y_{\text{hardness}} = -10.98 - 1522X_{405\text{nm}} + 1737X_{410\text{nm}} + 1326X_{460\text{nm}} - 1857X_{515\text{nm}} + 1025X_{560\text{nm}} - 1137X_{580\text{nm}} + 551X_{615\text{nm}} - 38X_{920\text{nm}} - 236X_{955\text{nm}} + 112X_{990\text{nm}} \quad (1)$$

$$Y_{\text{cohesiveness}} = 103 - 31.89X_{405\text{nm}} + 26.03X_{410\text{nm}} - 4.69X_{460\text{nm}} + 5.47X_{580\text{nm}} - 10.35X_{615\text{nm}} + 24.40X_{735\text{nm}} - 25.81X_{865\text{nm}} + 8.20X_{930\text{nm}} - 8.79X_{945\text{nm}} + 15.23X_{990\text{nm}} \quad (2)$$

$$Y_{\text{adhesiveness}} = 0.30 - 254.88X_{405\text{nm}} + 247.52X_{410\text{nm}} + 149.90X_{460\text{nm}} - 83.82X_{515\text{nm}} - 22.27X_{560\text{nm}} - 47.55X_{735\text{nm}} + 147.91X_{865\text{nm}} - 358.97X_{920\text{nm}} + 878.70X_{945\text{nm}} - 716.26X_{955\text{nm}} + 71.86X_{990\text{nm}} \quad (3)$$

$$Y_{\text{gumminess}} = -1 - 1129X_{405\text{nm}} + 1349X_{410\text{nm}} - 375X_{515\text{nm}} + 491X_{555\text{nm}} - 481X_{580\text{nm}} + 178X_{615\text{nm}} - 103X_{735\text{nm}} + 112X_{920\text{nm}} + 94X_{955\text{nm}} - 139X_{990\text{nm}} \quad (4)$$

$$Y_{\text{chewiness}} = -4 - 7313X_{405\text{nm}} + 8367X_{410\text{nm}} - 2345X_{515\text{nm}} + 3011X_{555\text{nm}} - 2983X_{580\text{nm}} + 1092X_{615\text{nm}} + 792X_{735\text{nm}} - 1068X_{920\text{nm}} + 606X_{945\text{nm}} - 489X_{990\text{nm}} \quad (5)$$

where $X_{i \text{ nm}}$ is the reflectance spectra at the wavelength of $i \text{ nm}$ and Y is the predicted TPA parameter. As shown in Table 3, the established MLR models with POW had similar results to the PLSR models (Method IV), where the average RMSECV value for five TPA parameters was increased by 2.31%.

In addition, besides the abovementioned two strategies (I and II) for image texture extraction, the extraction of image texture features was also conducted based on the selected optimal wavelengths (Naganathan et al., 2008a). In this study, the extraction of image texture features was conducted on POW (Strategy IV). There was no obvious difference between the results of PLSR models (Strategy I) and PLSR models (Strategy III) (data not shown). However the numbers of image texture features obtained in Strategy III were only about 10% of those in Strategy I. Actually, image textures are important features for texture detection of food products (Du & Sun, 2006; Zheng et al., 2006a, 2006b). It was found

Table 3
Performance of calibration models at optimal wavelengths (mean spectra of ROI in Spectral Set I) for predicting texture (hardness, adhesiveness, chewiness, cohesiveness, and gumminess) of salmon samples.

Method	Model	Texture	No. W ^a	No. of L ^b	Calibration		Cross-validation	
					r_c	RMSEC	r_{cv}	RMSECV
II	PLS ^c	Hardness	10	8	0.740	3.652	0.711	3.850
	PLS	Cohesiveness	9	8	0.576	0.065	0.500	0.069
	PLS	Adhesiveness	11	8	0.708	0.444	0.641	0.486
	PLS	Gumminess	10	8	0.761	1.681	0.717	1.821
	PLS	Chewiness	10	7	0.700	11.170	0.674	11.651
III	PLS	Hardness	14	9	0.740	3.656	0.664	4.098
	PLS	Cohesiveness	14	9	0.658	0.060	0.564	0.066
	PLS	Adhesiveness	14	8	0.680	0.461	0.629	0.493
	PLS	Gumminess	14	8	0.744	1.732	0.703	1.859
	PLS	Chewiness	14	9	0.735	10.610	0.658	11.874
IV	PLS	Hardness	10	8	0.740	3.652	0.711	3.850
	PLS	Cohesiveness	10	8	0.648	0.060	0.567	0.066
	PLS	Adhesiveness	11	10	0.712	0.441	0.639	0.488
	PLS	Gumminess	10	8	0.740	1.742	0.711	1.837
	PLS	Chewiness	10	8	0.735	10.597	0.702	11.226
IV	MLR ^d	Hardness	10	/	0.744	3.630	0.673	4.020
	MLR	Cohesiveness	10	/	0.657	0.060	0.563	0.066
	MLR	Adhesiveness	11	/	0.720	0.436	0.639	0.483
	MLR	Gumminess	10	/	0.742	1.738	0.670	1.925
	MLR	Chewiness	10	/	0.739	10.528	0.666	11.658

^a No. W: number of wavelengths.

^b No. L: number of latent variables.

^c PLSR: partial least square regression.

^d MLR: multiple linear regression.

that the texture of fish fillet is related to the diameter of the muscle fibres (Hatae, Yoshimatsu, & Matsumoto, 1990), which would be detectable by image textures. However, poor prediction results were obtained for the determination of TPA parameters based on any of the above three extraction strategies. The reason might be that due to the limitation of hardware in hyperspectral imaging systems, the resolution of acquired hyperspectral images is not high enough for the efficient extraction of image texture features compared to that of computer vision. In future, by considering the continuing improvement of the hardware capability of hyperspectral imaging system, it is anticipated that the extraction of image textures from hyperspectral images would be more efficient and hyperspectral imaging would become more powerful for the determination of TPA parameters of salmon fillets. As illustrated above, spectral features obtained better results than image texture features. Due to that MLR model is easier programed in an industrial on-line system than PLSR model, MLR models (Method IV) were considered as the best models for the determination of TPA parameters of salmon fillets.

3.5. Visualization of TPA parameters

As the final step of analyzing hyperspectral images, MLR models with the selected POW were used to visualize the distribution of TPA parameters. Fig. 3 demonstrates how the TPA parameters vary drastically between different parts in one sample. A large range of values was found in the same fillet, which shows salmon fillets had mixed constituents and non-uniform distribution of texture. Such variance depends on the distribution of fat, pigments and collagen (Casas, Martinez, Guillen, Pin, & Salmeron, 2006). It was noticeable that the sample depicted in Fig. 3 had obvious regions with high and low values for hardness, gumminess, and chewiness, while the distributions of cohesiveness and adhesiveness were more complex. The belly flap and dorsal areas had lower hardness, adhesiveness, gumminess, and chewiness values, and higher cohesiveness values. On the other hand, the middle parts of the fillets had lower cohesiveness values, and

higher hardness, adhesiveness, gumminess, and chewiness values. Although the difference of TPA parameters cannot be observed by visual inspection, the spatial distribution of these texture features within the salmon fillet could be discerned with the final distribution map which was generated by analysing the hyperspectral image of the sample. The generated distribution maps suggested that hyperspectral imaging with superior spatial information could provide more detailed information for measuring TPA parameters of salmon fillets rapidly and non-invasively than traditional universal testing machines that can only measure a few particular points of the sample destructively with a long measurement time.

4. Conclusions

Hyperspectral imaging technique in the spectral region of 400–1753 nm was applied for rapidly and non-invasively determining the distribution of texture in intact salmon fillets. The results obtained in this paper indicated that it was possible to use this rapid and non-invasive technique to determine the spatial distribution of several TPA parameters simultaneously. Spectral features had better prediction ability than image texture features in this study. A better prediction ability of image textures would be achieved by the improvement of hyperspectral imaging system to acquire images with high resolution. Spectral Set I in the visible and short-wave near infrared range of 400–1000 nm had better performance than Spectral Set II which covered the long-wave near infrared range of 967–1634 nm. Regression coefficients of PLSR models were used to choose optimal wavelengths for each TPA parameter (Method II). On the basis of the wavelengths selected by Method II, IOW and POW were further selected. Enhanced refinement of this technique via IOW will propel the development of a multispectral imaging system, which has a similar speed and cost of a RGB camera for process monitoring and real-time inspection. MLR equations for predicting TPA parameters were finally obtained based on POW to visualize the distribution maps of TPA parameters within salmon fillets. As the first research on rapid and non-invasive

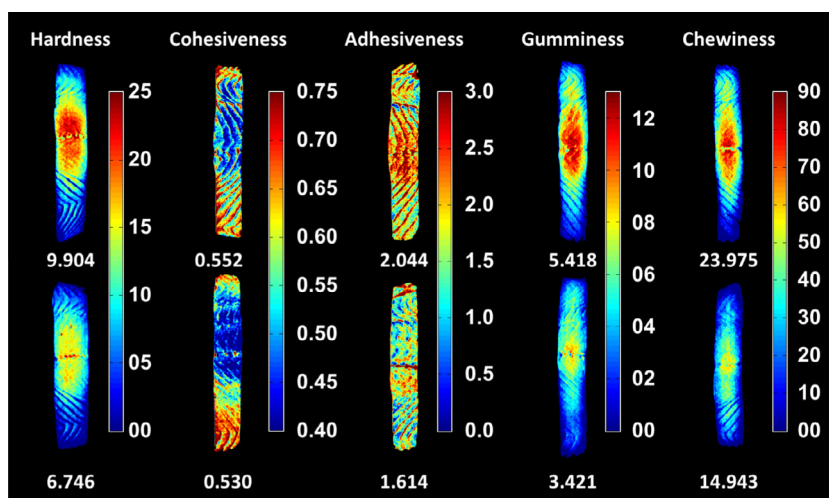


Fig. 3. Distribution maps of TPA parameters within salmon fillets.

determination of TPA distribution of food products, the results in this study are very promising and would promote more efforts on investigating hyperspectral imaging for forecasting TPA of salmon and other food products.

Acknowledgements

The authors would like to acknowledge the financial support provided by the Irish Research Council for Science, Engineering and Technology under the Government of Ireland Postdoctoral Fellowship scheme. We also thank Professor Colm O'Donnell for lending us the hyperspectral imaging equipment and Dr. Carlos Esquerre Feranandez for excellent technical assistance.

References

- Abdel-Nour, N., Ngadi, M., Prasher, S., & Karimi, Y. (2011). Prediction of egg freshness and albumen quality using visible/near infrared spectroscopy. *Food and Bioprocess Technology*, 4(5), 731–736.
- Antonucci, F., Pallottino, F., Paglia, G., Palma, A., D'Aquino, S., & Menesatti, P. (2011). Non-destructive estimation of mandarin maturity status through portable VIS-NIR spectrophotometer. *Food and Bioprocess Technology*, 4(5), 809–813.
- Ashton, T. J., Michie, I., & Johnston, I. A. (2010). A novel tensile test method to assess texture and gaping in salmon fillets. *Journal of Food Science*, 75(4), S182–S190.
- Berzaghi, P., & Riovanto, R. (2009). Near infrared spectroscopy in animal science production: Principles and applications. *Italian Journal of Animal Science*, 8, 39–62.
- Bourne, M. C. (2002). *Food texture and viscosity: Concept and measurement* (2nd ed.). New York: Academic Press.
- Casas, C., Martinez, O., Guillen, M. D., Pin, C., & Salmeron, J. (2006). Textural properties of raw Atlantic salmon (*Salmo salar*) at three points along the fillet, determined by different methods. *Food Control*, 17(7), 511–515.
- Chen, X. J., & Lei, X. X. (2009). Application of a hybrid variable selection method for determination of carbohydrate content in soy milk powder using visible and near infrared spectroscopy. *Journal of Agricultural and Food Chemistry*, 57(2), 334–340.
- Chen, X. J., Wu, D., He, Y., & Liu, S. (2011). Nondestructive differentiation of panax species using visible and shortwave near-infrared spectroscopy. *Food and Bioprocess Technology*, 4(5), 753–761.
- Clausi, D. A. (2002). An analysis of co-occurrence texture statistics as a function of grey level quantization. *Canadian Journal of Remote Sensing*, 28(1), 45–62.
- Du, C. J., & Sun, D.-W. (2005). Comparison of three methods for classification of pizza topping using different colour space transformations. *Journal of Food Engineering*, 68(3), 277–287.
- Du, C. J., & Sun, D.-W. (2006). Correlating image texture features extracted by five different methods with the tenderness of cooked pork ham: A feasibility study. *Transactions of the ASABE*, 49(2), 441–448.
- Dunajski, E. (1979). Texture of fish muscle. *Journal of Texture Studies*, 10(4), 301–318.
- ElMasry, G., Sun, D.-W., & Allen, P. (2012). Near-infrared hyperspectral imaging for predicting colour, pH and tenderness of fresh beef. *Journal of Food Engineering*, 110(1), 127–140.
- Francesca, A., Federico, P., Graziella, P., Amedeo, P., Salvatore, D., & Paolo, M. (2011). Non-destructive estimation of mandarin maturity status through portable VIS-NIR spectrophotometer. *Food and Bioprocess Technology*, 4(5), 809–813.
- Haralick, R. M., Shanmuga, K., & Dinstein, I. (1973). Textural features for image classification. *IEEE Transactions on Systems Man and Cybernetics, SMC*, 3(6), 610–621.
- Hatae, K., Yoshimatsu, F., & Matsumoto, J. J. (1990). Role of muscle-fibers in contributing firmness of cooked fish. *Journal of Food Science*, 55(3), 693–696.
- He, H.-J., Wu, D., & Sun, D.-W. (2013). Non-destructive and rapid analysis of moisture distribution in farmed Atlantic salmon (*Salmo salar*) fillets using visible and near-infrared hyperspectral imaging. *Innovative Food Science and Emerging Technologies*. <http://dx.doi.org/10.1016/j.ifset.2013.02.009>. in press.
- Hu, X. P., Toyoda, K., Yamanoue, M., Ihara, I., & Nakai, K. (2010). Evaluation of fatty acid profile of Wagyu beef by ATR-FTIR spectroscopy. *Food and Bioprocess Technology*, 3(6), 883–891.
- Isaksson, T., Swensen, L. P., Taylor, R. G., Fjaera, S. O., & Skjervold, P. O. (2002). Non-destructive texture analysis of farmed Atlantic salmon using visual/near-infrared reflectance spectroscopy. *Journal of the Science of Food and Agriculture*, 82(1), 53–60.
- Jackman, P., Sun, D.-W., Du, C.-J., & Allen, P. (2008). Prediction of beef eating quality from colour, marbling and wavelet texture features. *Meat Science*, 80(4), 1273–1281.
- Jackman, P., Sun, D.-W., Du, C.-J., & Allen, P. (2009). Prediction of beef eating qualities from colour, marbling and wavelet surface texture features using homogenous carcass treatment. *Pattern Recognition*, 42(5), 751–763.
- Jonsson, A., Sigurgisladottir, S., Hafsteinsson, H., & Kristbergsson, K. (2001). Textural properties of raw Atlantic salmon (*Salmo salar*) fillets measured by different methods in comparison to expressible moisture. *Aquaculture Nutrition*, 7(2), 81–89.
- Lorente, D., Aleixos, N., Gómez-Sanchis, J., Cubero, S., & Blasco, J. (2013). Selection of optimal wavelength features for decay detection in citrus fruit using the ROC curve and neural networks. *Food and Bioprocess Technology*, 6, 530–541.
- Lorente, D., Aleixos, N., Gomez-Sanchis, J., Cubero, S., Garcia-Navarrete, O. L., & Blasco, J. (2012). Recent advances and applications of hyperspectral imaging for fruit and vegetable quality assessment. *Food and Bioprocess Technology*, 5(4), 1121–1142.
- Morkore, T., & Einen, O. (2003). Relating sensory and instrumental texture analyses of Atlantic salmon. *Journal of Food Science*, 68(4), 1492–1497.
- Naganathan, G. K., Grimes, L. M., Subbiah, J., Calkins, C. R., Samal, A., & Meyer, G. E. (2008a). Partial least squares analysis of near-infrared hyperspectral images for beef tenderness prediction. *Sensing and Instrumentation for Food Quality and Safety*, 2, 178–188.
- Naganathan, G. K., Grimes, L. M., Subbiah, J., Calkins, C. R., Samal, A., & Meyer, G. E. (2008b). Visible/near-infrared hyperspectral imaging for beef tenderness prediction. *Computers and Electronics in Agriculture*, 64(2), 225–233.
- Reeves, J. III, (1994). Effects of water on the spectra of model compounds in the short-wavelength near infrared spectral region (14,000–9091 cm⁻¹ or 714–1100 nm). *Journal of Near Infrared Spectroscopy*, 2(4), 199–212.
- Sigurgisladottir, S., Hafsteinsson, H., Jonsson, A., Lie, O., Nortvedt, R., Thomassen, M., et al. (1999). Textural properties of raw salmon fillets as related to sampling method. *Journal of Food Science*, 64(1), 99–104.
- Sinija, V., & Mishra, H. (2011). FTNIR spectroscopic method for determination of moisture content in green tea granules. *Food and Bioprocess Technology*, 4(1), 136–141.
- Soh, L. K., & Tsatsoulis, C. (1999). Texture analysis of SAR sea ice imagery using gray level co-occurrence matrices. *IEEE Transactions on Geoscience and Remote Sensing*, 37(2), 780–795.

- Sun, D.-W., & Brosnan, T. (2003). Pizza quality evaluation using computer vision - part 1 - Pizza base and sauce spread. *Journal of Food Engineering*, 57(1), 81–89.
- Umbaugh, S. E. (2010). *Digital imaging processing and analysis: Human and computer vision applications with CVIPtools* (2nd ed.). Boca Raton, FL: CRC Press.
- Valous, N. A., Mendoza, F., Sun, D.-W., & Allen, P. (2009). Colour calibration of a laboratory computer vision system for quality evaluation of pre-sliced hams. *Meat Science*, 81(1), 132–141.
- Veland, J. O., & Torrisen, O. J. (1999). The texture of Atlantic salmon (*Salmo salar*) muscle as measured instrumentally using TPA and Warner–Brazler shear test. *Journal of the Science of Food and Agriculture*, 79(12), 1737–1746.
- Wang, H. H., & Sun, D.-W. (2002). Melting characteristics of cheese: analysis of effect of cheese dimensions using computer vision techniques. *Journal of Food Engineering*, 52(3), 279–284.
- Wu, D., Chen, X., Zhu, X., Guan, X., & Wu, G. (2011). Uninformative variable elimination for improvement of successive projections algorithm on spectral multivariable selection with different calibration algorithms for the rapid and non-destructive determination of protein content in dried laver. *Analytical Methods*, 3(8), 1790–1796.
- Wu, D., Feng, L., He, Y., & Bao, Y. (2008a). Variety identification of Chinese cabbage seeds using visible and near-infrared spectroscopy. *Transactions of the ASABE*, 51(6), 2193–2199.
- Wu, D., He, Y., Feng, S. J., & Sun, D.-W. (2008b). Study on infrared spectroscopy technique for fast measurement of protein content in milk powder based on LS-SVM. *Journal of Food Engineering*, 84(1), 124–131.
- Wu, D., He, Y., Nie, P. C., Cao, F., & Bao, Y. D. (2010). Hybrid variable selection in visible and near-infrared spectral analysis for non-invasive quality determination of grape juice. *Analytica Chimica Acta*, 659(1–2), 229–237.
- Wu, D., He, Y., Shi, J. H., & Feng, S. J. (2009). Exploring near and mid infrared spectroscopy to predict trace iron and zinc contents in powdered milk. *Journal of Agricultural and Food Chemistry*, 57(5), 1697–1704.
- Wu, D., Nie, P. C., Cuello, J., He, Y., Wang, Z. P., & Wu, H. X. (2011). Application of visible and near infrared spectroscopy for rapid and non-invasive quantification of common adulterants in *Spirulina* powder. *Journal of Food Engineering*, 102(3), 278–286.
- Wu, D., Nie, P. C., He, Y., & Bao, Y. D. (2012a). Determination of calcium content in powdered milk using near and mid-infrared spectroscopy with variable selection and chemometrics. *Food and Bioprocess Technology*, 5(4), 1402–1410.
- Wu, D., Shi, H., Wang, S., He, Y., Bao, Y., & Liu, K. (2012b). Rapid prediction of moisture content of dehydrated prawns using online hyperspectral imaging system. *Analytica Chimica Acta*, 726, 57–66.
- Wu, D., Wang, S., Wang, N., Nie, P., He, Y., Sun, D.-W., et al. (2013). Application of time series-hyperspectral imaging (TS-HSI) for determining water distribution within beef and spectral kinetic analysis during dehydration. *Food and Bioprocess Technology*. <http://dx.doi.org/10.1007/s11947-012-0928-0>. in press.
- Zheng, C., Sun, D.-W., & Zheng, L. (2006a). Classification of tenderness of large cooked beef joints using wavelet and Gabor textural features. *Transactions of the ASABE*, 49(5), 1447–1454.
- Zheng, C. X., Sun, D.-W., & Zheng, L. Y. (2006b). Recent applications of image texture for evaluation of food qualities – A review. *Trends in Food Science and Technology*, 17(3), 113–128.